The effect of railway local irregularities on ground vibration

Available online at www.sciencedirect.com

ScienceDirect

Transportation Research — Part D: Transport and Environment 00 (2015) 1–17

The effect of railway local irregularities on ground vibration

Georges Kouroussis[1], David P. Connolly[2], Georgios Alexandrou[1], and Konstantinos Vogiatzis[3]

1 *University of Mons — UMONS, Faculty of Engineering, Department of Theoretical Mechanics, Dynamics and Vibrations, Place du Parc 20, B-7000 Mons, Belgium*

2 *Heriot-Watt University, School of Energy, Geoscience, Infrastructure & Society, Edinburgh EH14 4AS, United Kingdom*

3 *University of Thessaly, School of the Civil Engineering, Pedion Areos, 383 34 Volos, Greece*

Abstract

The environmental effects of ground-borne vibrations generated due to localised railway defects is a growing concern in urban areas. Frequency domain modelling approaches are well suited for predicting vibration levels on standard railway lines due to track periodicity. However, when considering individual, non-periodic, localised defects (e.g. a rail joint), frequency domain modelling becomes challenging. Therefore in this study, a previously validated, time domain, three-dimensional ground vibration prediction model is modified to analyse such defects. A range of different local (discontinuous) rail and wheel irregularity are mathematically modelled, including: rail joints, switches, crossings and wheel flats. Each is investigated using a sensitivity analysis, where defect size and vehicle speed is varied. To quantify the effect on railroad ground-borne vibration levels, a variety of exposure-response relationships are analysed, including: peak particle velocity, maximum weighted time-averaged velocity and weighted decibel velocity. It is shown that local irregularities cause a significant increase in vibration in comparison to a smooth track, and that the vibrations can propagate to greater distances from the line. Furthermore, the results show that step-down joints generate the highest levels of vibration, whereas wheel flats generate much lower levels. It is also found that defect size influences vibration levels, and larger defects cause greater vibration. Lastly, it is shown that for different defect types, train speed effects are complex, and may cause either an increase or decrease in vibration levels.

Keywords:
wheel/rail impact; vehicle/track interaction; railroad ground-borne vibration; environmental impact assessment; flat wheel; local track irregularities

1. Introduction

Railway induced ground vibrations can cause negative effects on urban environments situated near rail lines. The propagation of railway vibrations (particularly in urban areas) is complex, due to the different transmission paths within a medium that is fundamentally inhomogeneous, non-engineered and infinite in three directions. There is a large body of research into railway-induced ground vibrations, such as their effect on urban environments and potential mitigation measures (e.g. wave impeding blocks (Coulier et al., 2013), trenches (Connolly, Giannopoulos, Fan, Woodward and Forde, 2013) or

Email address: georges.kouroussis@umons.ac.be (Georges Kouroussis[1])

wave barrier (Garinei et al., 2014)). Furthermore, for high-speed trains (Degrande and Schillemans, 2001; Galvín and Domínguez, 2009; Costa et al., 2010; Connolly et al., 2015), research is currently motivated by the so-called "supercritical phenomenon" which occurs when the vehicle speed is close to the Rayleigh ground wave speed. Critical speed depends on the soil flexibility and may be close to that of conventional high-speed lines (Madshus and Kaynia, 2000; Connolly, Kouroussis, Laghrouche, Ho and Forde, 2014). Despite the large vibration levels generated by these lines which are underlain by soft soils (Connolly, Kouroussis, Woodward, Costa, Verlinden and Forde, 2014), the distance d between the track and neighbouring structures is relatively high and the vibration attenuates rapidly. In the case of railway traffic, the attenuation is associated with a power law of the form d^{-q}, where q lies between 0.5 and 1.1, depending on the soil configuration (Auersch and Said, 2010). Connolly, Kouroussis, Woodward, Verlinden, Giannopoulos and Forde (2014) proposed that it is possible to establish relationships between six key railway variables for ground vibration metrics in the case of high-speed lines. The situation is significantly different for the case of urban transit, because:

- The distance d between track and building is relatively close.
- The contribution of the vehicle weight and speed (quasi-static effects) is low.
- The presence of local defects induces elevated localised vibrations (dynamic effects).

Local defects are a significant source of dynamic excitation on railway tracks. Accurate descriptions of the interaction between the track and the vehicle have been modelled by Nielsen and Abrahamsson (1992), Zhai and Sun (1994); Zhai et al. (2013) and Oscarsson and Dahlberg (1998); Andersson and Oscarsson (1999). They take into account the different elements of the track/foundation system. Similar research was also undertaken by Kouroussis et al. (2011) to show that an accurate simulation of track/soil interaction is important in the prediction of ground-borne vibration (Kouroussis and Verlinden, 2015). These numerical approaches offer the possibility of studying local defect effects on track dynamics. Indeed, the study of vehicle/track coupling with local defects is of growing interest. The influence of vehicle-flexible mode shapes on the ride quality has been investigated (Younesian et al., 2014), including singular geometrical imperfections. Mandal et al. (2014) propose simplified equations for the impact forces on wheels caused by permanently dipped rail joints; these elevated forces are characterised by high-frequency content in comparison to the typical static excitation, and occur for a very short duration. Uzzal et al. (2014) considered the dynamic impact response due to the presence of multiple wheel flats, for different sizes and relative positions of flat spots. Zhao et al. (2012) employed a three-dimensional finite element model to evaluate the wheel/rail impact forces at local rail surface defect zones. They also evaluated the resulting dynamic forces at the discrete supports of the rail under different train speeds. Grossoni et al. (2015) proposed a parametric study to understand the dynamic behaviour of a rail joint and the influence of track and vehicle parameters.

The aforementioned studies focus on the track/vehicle response however only a small number of studies have analysed the effect of local defects on ground vibration. Despite this, many ground-borne vibration complaints in urban environments are due to local rail and wheel surface defects (e.g. switches, rail joints, ...). Kouroussis, Pauwels, Brux, Conti and Verlinden (2014) quantified the vibration generated by a tram in the presence of a local rail defect using a numerical model in two successive steps. Using the same approach, Alexandrou et al. (2015) also studied the wheel flat effect on ground motion and analysed the influence of wheel flat size. In addition, Vogiatzis (2010; 2012) undertook a large-scale analysis of ground vibrations generated by underground Athens metro lines by studying wheel flat impact forces as impulses. Mitigations solutions were proposed by improving vehicle and track design, such as reduction in unsprung mass minimizing wheel polygonalisation or wheel flat (Nielsen et al., 2015), creating transition zones to avoid abrupt changes in the track's vertical stiffness (Paixão et al., 2015) or lift-over crossings to minimise vibrations in sensitive buildings (Talbot, 2014).

As the source of vibration is the wheel/rail contact, it is essential to study vehicle interaction with the track and the soil. Therefore, Costa et al. (2012) showed the importance of integrating a multibody model of the vehicle with the track/soil simulations and that in the case of a distributed

rail's unevenness, sprung masses have minimal effects on the ground vibration motion. Furthermore, Kouroussis, Connolly and Verlinden (2014) concluded that the choice between a simple or detailed model for the vehicle depends upon the importance of wheel and rail unevenness. This is because transient vibration generated at rail or wheel discontinuities is not comparable to the continuous vibration due to wheel/rail roughness.

This paper analyses the effect of typical local rail and wheel surface defects as shown in Figure 1. First, a general description of the prediction model, based on a numerical two-step approach, is presented. A validated (Kouroussis et al., 2015) vehicle-track-soil model is studied, based on the AM96 trainset, largely used in Brussels Region (Belgium), for which substantial measured data exists (Kouroussis, Conti and Verlinden, 2013). Different defect geometries and sizes are considered for various train speeds and then their effect on vibration levels analysed.

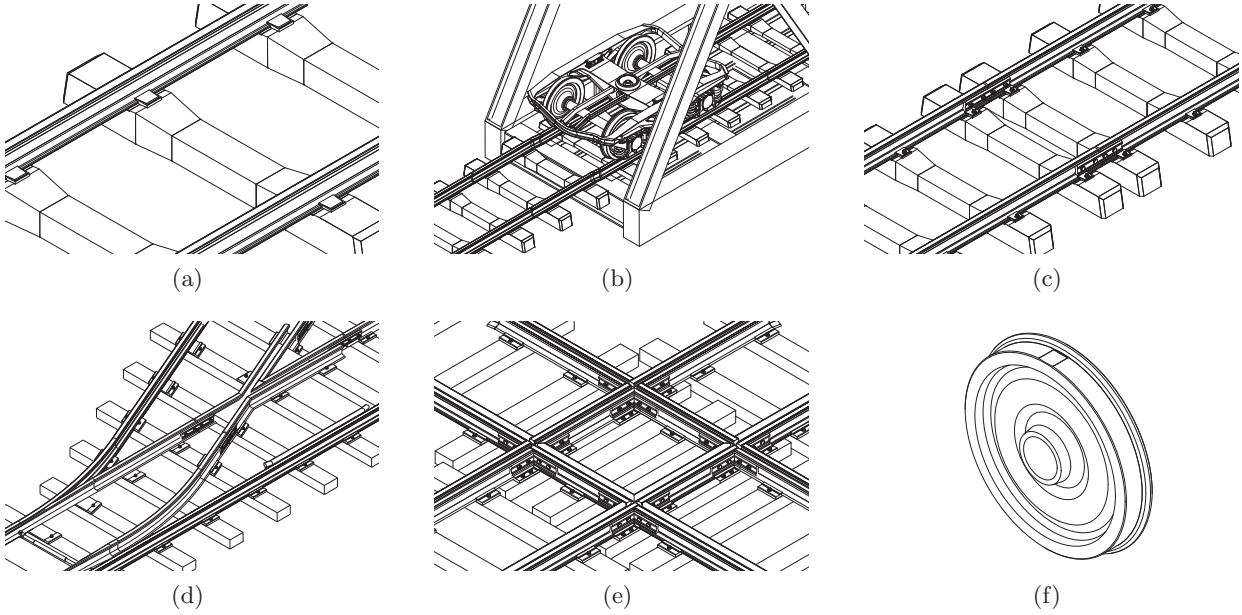

Figure 1. Overview of possible surface defects encountered in practice: (a) reference (no defect), (b) foundation transition, (c) fishplated rail joints, (d) turnout, (e) crossing and (f) wheel flat.

2. Classification of local defects

Figure 2 shows the local rail and wheel surface defect geometries associated with the defects illustrated in Figure 1. For each defect, the geometry and the shape "seen" by the wheel/rail interface are illustrated. The shape seen accounts for the wheel radius R_w and the vehicle speed v_0.

The link between these theoretical shapes (Figure 2) and the physical defects that are present on track is not a one-to-one relationship. Instead, real defects may form a combination of the defects shown. Despite this, some typical cases can be considered:

- Complete switch mechanism (Figure 1(d)) comprises successive step-up joints and pulse joints, e.g. Figure 2(b) and Figure 2(e).
- Crossings, and diamond crossings as presented in Figure 1(e), are used in double junction and are often found on tram or streetcar networks where lines cross or split. They are considered as a first approximation as two successive negative pulse joints (Figure 2(e)).

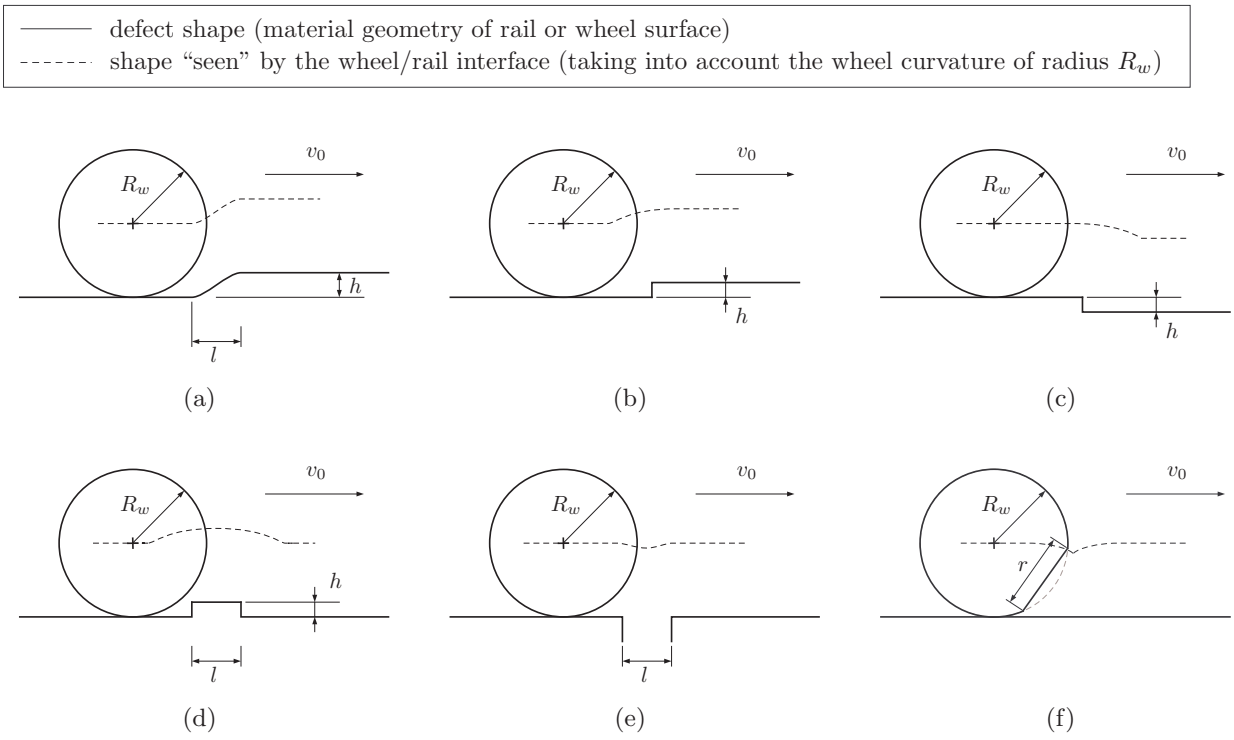

Figure 2. Mathematical modelling of local rail and wheel surface defects: (a) ramp, (b) step-up joint, (c) step-down joint, (d) pulse joint, (e) negative pulse joint and (f) wheel flat.

- Foundation transition zone (Figure 1(b)) is similar to a ramp which may occur at track–bridge or ballast–slab track transitions due to a change in track stiffness (Figure 2(a)). A local foundation compaction can induce a variation in height of rail.
- Rail joint (Figure 1(c)) can comprise of any combination of Figures 2(b)–(e). This is dependent upon the variation in height and in spacing between the two connected rails.
- Wheel flat (Figure 1(f)) is considered as a newly created flat, Figure 2(f).

3. Numerical model

3.1. Fundamental assumptions

The proposed prediction model is based on two successive calculations and thus facilitates a high accuracy modelling approach for each subsystem. The first step is a vehicle/track analysis. The ballast reactions are then saved and used as input forces for the second step which is a ground wave model. The following assumptions are made:

- Only rigid (multi-)body modes are considered for the vehicle.
- Only vertical dynamic forces are analysed. The vehicle/track model is defined as a bidimensional problem (in the vertical plane); all the proposed defects are assumed to be symmetrical on each side of the track and in-phase.
- The track can be modelled using a three-layer track model, including the foundation.

- To couple the vehicle and track equations of motion, normal wheel/rail contacts must be expressed. Therefore, the corresponding contact forces are calculated according to non-linear Hertz's theory. The track and wheel imperfections are included in the contact law.
- At the transition zones (e.g. between the wheel curvature and wheel flat), a small radius is modelled for the corner between the two profiles, with a value of $0.01\,R_w$ to avoid singularities in the contact zones.
- The vehicle has a constant speed v_0 for all presented cases.

For the soil modelling, novel soil modelling approaches (e.g. 2.5D modelling (Sheng et al., 2006; Costa et al., 2010; Galvín et al., 2010) and Floquet transforms (Chebli et al., 2008)) are unfeasible due to non-periodicity in the track direction. A three-dimensional approach is therefore necessary.

3.2. Vehicle/track modelling

The dynamics of the vehicle/track subsystem are simulated by considering a multibody vehicle model moving on a flexible track (Figure 3). The wheel/rail forces are defined using Hertz's theory and allow coupling between the vehicle model and the track. The latter is defined as a flexible beam discretely supported by the sleepers, including viscoelastic elements for the ballast and the railpads. To take into account the dynamic behaviour of the foundation (which plays an important role at low frequencies), a coupled lumped mass model is added to the track model with interconnection elements for the foundation-to-foundation coupling (Kouroussis, Van Parys, Conti and Verlinden, 2013). This model does not take into account other track degrees of freedom. In particular, the sleeper is known to move in a translational and rotational displacements which would expect to produce a more complex excitation. With that in mind, the proposed model is a reasonable approach to take for the study being presented, since it was validated in similar cases (Kouroussis et al., 2012). A C++ object-oriented program was developed using the in-house EasyDyn library (Verlinden et al., 2013). An application based on a MuPad/Xcas platform generates symbolic kinematic expressions for the vehicle. The generalized coordinates approach enables a system of pure ordinary differential equations, without constraint equations. The MuPad/Xcas platform creates a C++ code directly compilable with the EasyDyn library. This programmable code is completed by the definition of applied forces (suspensions, wheel/rail contact) and the link to the track model (which is already established and depends only on site parameters). An implicit scheme is used for the simulation in this first step due to the stiff equations partially obtained for the wheel/rail contact.

3.3. Wheel/rail contact

To couple the vehicle and track equations of motion, normal wheel/rail contacts must be expressed. The corresponding contact forces are calculated according to Hertz's non-linear theory. The vertical dynamic forces released by the contact and that act upon each wheel i and on the rail at the coordinate x_j can be written as:

$$F_{\text{rail/wheel},i} = \begin{cases} -K_{Hz}\left(z_{\text{wheel},i} - z_{\text{rail}}(x_j) - h_{\text{defect}}(x_j)\right)^{3/2} \\ \text{if } z_{\text{wheel},i} > \left(z_{\text{rail}}(x_j) - h_{\text{defect}}(x_j)\right) \\ 0 \qquad \text{otherwise} \end{cases} \tag{1}$$

$$= -F_{\text{wheel},i/\text{rail}} \tag{2}$$

where K_{Hz} is determined from the radii of curvature of the wheel and rail surfaces and the elastic properties of their materials. $z_{\text{wheel},i}$ and $z_{\text{rail}}(x_j)$ denote the vertical positions of the wheel and of the rail, respectively. As the vehicle moves along the track at a specific speed v_0, the rail contact point changes. The defect geometry h_{defect} is calculated from the mathematical shapes defined in Section 2. A 3D finite element model is first employed to simulate rail and wheel stress and strain distributions in the wheel/rail contact to determine the values of K_{Hz}.

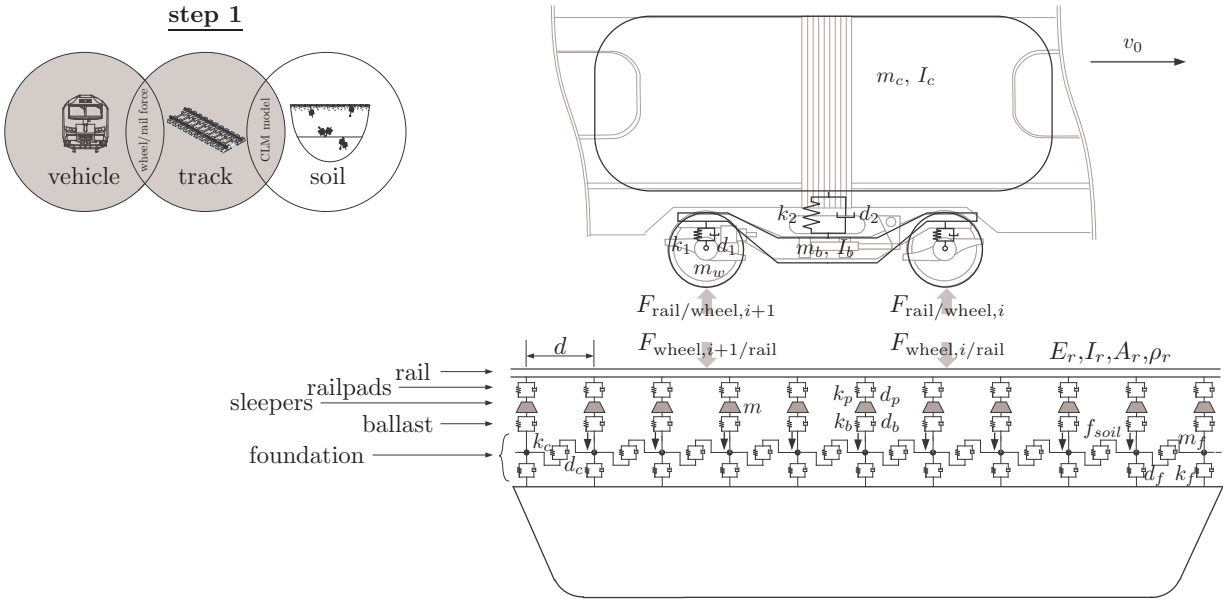

Figure 3. Description of the prediction model: vehicle/track/foundation simulation.

3.4. Ground wave propagation modelling

The second step addresses the dynamics of the soil subsystem. Soil surface forces f_{soil} represent the contribution from the sleepers (Figure 4). The dynamic ground response is calculated using finite element methods via the commercial software package ABAQUS. Kouroussis, Van Parys, Conti and Verlinden (2014) implemented a fully 3D finite element model to optimise finite element method performance and to allow treatment of complex geometry (track embankment, inclined layer interfaces). Moreover, variability in track profile and high ground vibrations originating in singular rail surface defects can be readily analysed. The combined use of viscous boundaries and infinite elements provides more efficient non-reflecting conditions than classical setups (free or fixed boundaries). Here, the small dependence on incident wave angle and dynamic parameters was quantitatively carried out for each solution. A spherical soil border geometry is defined, to which infinite elements are attached. This convex-shape configuration ensures the condition of non-crossing infinite elements. The simulation is performed in the time domain. This is an interesting solution to study ground vibrations in a relatively small area of interest. Since ground vibrations are inherently a transient phenomenon, the time domain analysis is appropriate to simulate wave propagation. It also does not impose any condition on the domain size, which would be required in the frequency domain. Moreover, the equations of motion describing the soil dynamics use an explicit central difference integration scheme to reduce computational burden.

3.5. Environmental impact assessment

A selection of standards/metrics used in Europe and North America were chosen to quantify the influence of vibrations on human perception and damages to buildings (Kouroussis, Conti and Verlinden, 2014), in the range of 1–80 Hz.

ISO standard (International Organization for Standardization, 2003) is dedicated to vibrations felt within a building. In 2013, the evaluation procedure was updated to include frequency-dependent filters related to activity, but was independent of measurement direction and human position (standing, sitting or sleeping). The previous 1989 version of ISO 2631-2 is based on a comparison of the frequency signal with a third-octave band limit curve. The weighted acceleration a_w is derived from the time history of ground vibration acceleration $a(t)$. A root-mean squared (rms) value is calculated and used to describe the steady

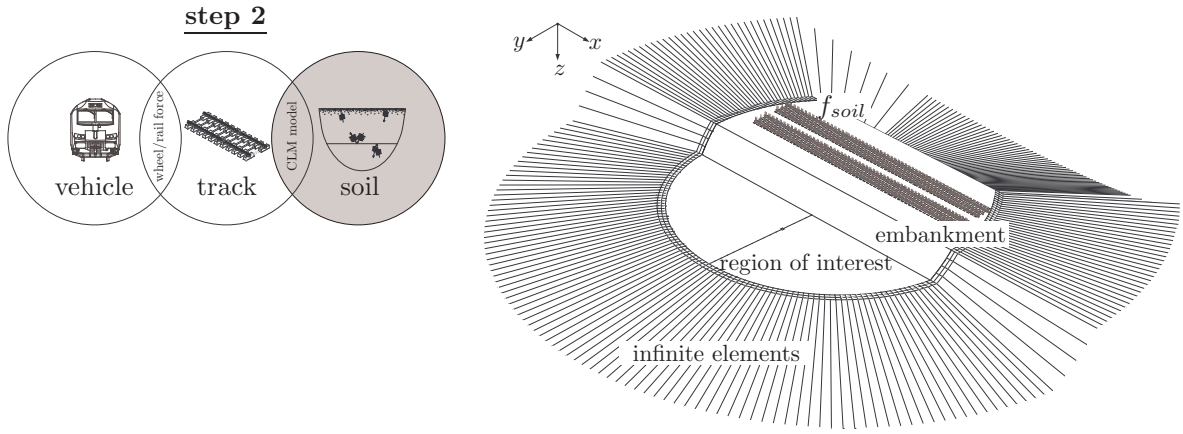

Figure 4. Finite element soil modelling using infinite elements and viscous boundary conditions.

vibration amplitude, assuming that the human body responds to an average vibration amplitude between a recorded time of $0 \leq t \leq T$

$$\langle a_w \rangle = \sqrt{\frac{1}{T} \int_0^T a_w^2(t)\, \mathrm{d}t} \ . \tag{3}$$

Guidelines on the effect of vibration on comfort and perception are provided and limits are used to define vibration thresholds.

Alternatively, as vibration is often non-stationary, DIN 4150-2 standard (Deutsches Institut für Normung, 1999a) proposes the use of a running, root-mean square applied to the velocity signal. A weighted, time-averaged signal is defined by:

$$KB_F(t) = \sqrt{\frac{1}{\tau} \int_0^t KB^2(\xi)\, e^{-\frac{t-\xi}{\tau}}\, \mathrm{d}\xi} \tag{4}$$

where the weighted velocity signal $KB(t)$ is obtained by passing the original ground vibration velocity signal $v(t)$ through the high-pass filter

$$H_{KB}(f) = \frac{1}{\sqrt{1 + (5.6/f)^2}} \ . \tag{5}$$

The filter is a function of the frequency f. The assimilation time τ is typically equal to 0.125 s, which takes into account transient phenomena, such as impacts or shocks, that would otherwise be masked if a simple operation is performed. The only comfort that can then be assessed is by comparing the maximum level $KB_{F,\max}$ with three guideline limits denoted by A_u, A_o and A_r. Part 3 of DIN 4150-3 (Deutsches Institut für Normung, 1999b) is entirely dedicated to structural vibrations. The peak particle velocity PPV, which is defined as the maximum absolute amplitude of the velocity time signal, is calculated and compared to other limits, dependent upon the dominant signal frequency. If multiple directions are measured, the maximum of the three components (x, y or z) is

$$PPV = \max(|v_x|, |v_y|, |v_z|) \ . \tag{6}$$

In addition to Eq. (6), when the three components are of the same order of magnitude, the norm of the vector velocity can be used, as suggested by the Swiss standard (Schweizerische Normen-Vereinigung, 1992)

$$PPV = \sqrt{v_x^2 + v_y^2 + v_z^2} \ . \tag{7}$$

Taking into account that vibrations exist over a wide range of amplitudes, the U.S. Department of Transportation adopted a decibel scale in order to evaluate the vibrational impact of a passing high-speed train (U. S. Department of Transportation, 1998). This is similar to how noise is measured and compresses the range of numbers required to describe the vibration velocity level. It is defined as:

$$V_{dB} = 20 \log_{10} \frac{v_{rms}}{5\,10^{-8}_{[\mathrm{m/s}]}} \tag{8}$$

where v_{rms} is the root mean square amplitude of the velocity time history. Note that no weighting is applied to the signal, which is contrary to ISO standards.

4. Numerical simulations and results

Local defects are often encountered by urban trains. Therefore, this study focuses on the InterCity train operating in Brussels (Belgium). The AM96 trainset, largely used by the Belgian Railway Operator, SNCB, is typically used for InterCity and InterRegion connections. This study evaluates the AM96 trainset's generation of elevated ground vibration levels in comparison to other domestic trains (Kouroussis, Conti and Verlinden, 2013). It consists of three carriages, designated HVBX, HVB, and HVADX. The HVBX leading wagon is equipped with motorised bogies, whereas the HVB (middle) and HVADX (end) wagons are trailer carriages. Figure 5 shows the configurations and the positions of each wheelset on the vehicle. A classical multibody approach is used and limits the vehicle dynamics to pitch and bounce motions. Table 1 presents the dynamic and geometrical informations of each carriage. Track and soil data are provided in Tables 2 and 3, respectively. This vehicle configuration has been recently validated using free field measurements (Kouroussis et al., 2015).

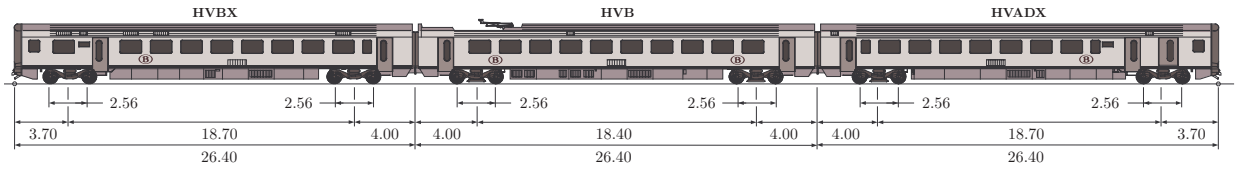

Figure 5. Configuration of the AM96 electric multiple unit.

Table 1. Dynamic parameters of AM96 vehicle — unladen weight (Kouroussis, Connolly and Verlinden, 2014).

	HVB	HVADX	HVBX
Car body mass	25200 kg	28900 kg	25932 kg
Bogie mass	6900 kg	7050 kg	11800 kg
Wheelset mass	1700 kg	1700 kg	2375 kg
Car body radius of gyration	7.09 m	7.09 m	7.09 m
Bogie radius of gyration	0.47 m	0.47 m	0.47 m
Bogie spacing	15.84 m	15.84 m	15.84 m
Wheelset spacing	2.56 m	2.56 m	2.56 m
Primary suspension stiffness	1.30 MN/m	1.30 MN/m	1.81 MN/m
Primary suspension damping	3.7 kNs/m	3.7 kNs/m	1.14 kNs/m
Secondary suspension stiffness	0.69 MN/m	0.69 MN/m	0.69 MN/m
Secondary suspension damping	22.6 kNs/m	22.6 kNs/m	14 kNs/m

Table 2. Parameters of the track at Watermael (Brussels Region — Belgium).

Rail flexural stiffness	$6.42\,\mathrm{MNm^2}$
Rail mass per length	$60\,\mathrm{kg/m}$
Sleeper spacing	$0.6\,\mathrm{m}$
Sleeper mass	$150\,\mathrm{kg}$
Railpad stiffness	$550\,\mathrm{MN/m}$
Railpad damping coefficient	$68\,\mathrm{kNs/m}$
Ballast stiffness	$361\,\mathrm{MN/m}$
Ballast damping coefficient	$55\,\mathrm{kNs/m}$

Table 3. Summary of the dynamic soil characteristics at site of Watermael (Brussels Region — Belgium).

Layer	top	bottom
Young's modulus	$120\,\mathrm{MN/m^2}$	$500\,\mathrm{MN/m^2}$
Density	$1600\,\mathrm{kg/m^3}$	$2500\,\mathrm{kg/m^3}$
Poisson's ratio	0.3	0.3
Compression wave velocity	$320\,\mathrm{m/s}$	$520\,\mathrm{m/s}$
Shear wave velocity	$171\,\mathrm{m/s}$	$278\,\mathrm{m/s}$
Viscous damping	$0.0004\,\mathrm{s}$	$0.0004\,\mathrm{s}$

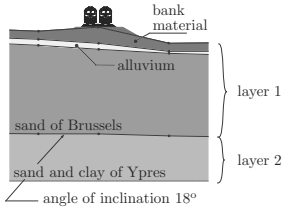

4.1. Free-field ground vibrations

Figure 6 presents numerical results, for the case of no defect and also a ramp irregularity (vertical height $h = 5\,\mathrm{mm}$ and horizontal length $l = 200\,\mathrm{mm}$). The AM96 trainset runs at a speed v_0 of $120\,\mathrm{km/h}$. The comparison is based on the time history of numerical velocities in the vertical direction (Figure 6(a)) and the corresponding normalized frequency content (Figure 6(b)), both for a distance of $10\,\mathrm{m}$ from the track. A significant difference in levels is observed between the two cases' velocity traces (more than ten times magnification), thus showing the significant contribution of local irregularities to vibration levels. The passing of each wheelset is more clearly pronounced in the case where the defect is present.

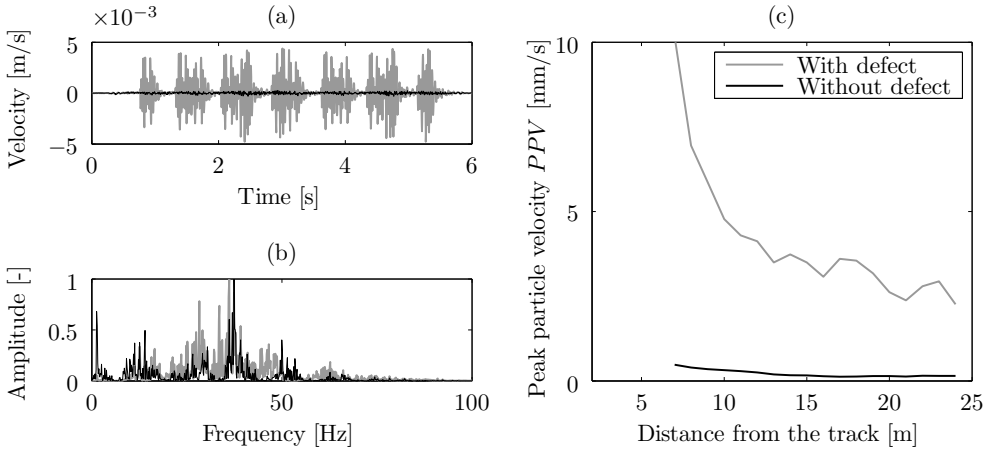

Figure 6. Comparison between numerical data (grey: with 5 mm height/200 mm length ramp defect; black: without defect) related to the passage of an AM96 trainset (2×3 carriages) at a speed v_0 of 120 km/h: (a) time histories at 10 m from the track, (b) normalised frequency contents at 10 m from the track and (c) peak particle velocity as a function of the distance from the track.

Figure 6(b) shows that, although the frequency content is spread over the range [0;100 Hz], all dominant

frequencies are located in the frequency range 0 – 60 Hz. Several dominant frequencies due to the fundamental and harmonic carriage frequencies are present and are a multiple of

$$f_c = \frac{v_0}{L_c} \tag{9}$$

where L_c is the carriage length. In addition, the fundamental axle and bogie passage frequencies imply a double amplitude modulation, as discussed in (Kouroussis, Connolly and Verlinden, 2014):

$$f_a = \frac{v_0}{L_a} \tag{10}$$

$$f_b = \frac{v_0}{L_b} \tag{11}$$

where L_a is the wheelset spacing, and L_b the bogie spacing. In the studied case ($f_a = 13$ Hz and $f_b = 1.8$ Hz), the axle frequency modulation is clearly visible on both spectra (i.e. at 6.5 Hz, 19.5 Hz, 32.5 Hz, 45.5 Hz and 58.5 Hz where the magnitude is close to zero). This modulation effect is also visible on the dominant frequencies $n\,f_c$. More importantly, it is seen that the presence of the local defect amplifies the frequency magnitude between 20 Hz and 60 Hz. In this large range, the soil resonance also plays a role (Kouroussis et al., 2015).

Figure 6(c) shows the far field peak particle velocity PPV defined by Eq. (6). The analysis is based on a track with an embankment: receivers are placed outside the embankment area (in the far field) where ground vibration is most likely problematic. The ground vibration level decreases with the distance d from the track and the decay rate is different when the defect is present. Without the defect it is approximately $d^{-0.9}$; however, with the defect, it reaches up $d^{-1.2}$. Interestingly, the decay rate is then outside the power law range [0.5–1.1] proposed by Auersch and Said (2010).

Figure 7 shows a cross section of the ground wave propagation for the same defect case, thus giving a comprehensive view of the free field response on the soil's surface. The selected time histories show the instants when the first bogie crosses the local defect (beginning of the ramp). At $t < 0.75$ s, the ground wave generation is due to the quasi-static contribution of the vehicle (no contact with the local defect). At $t > 0.75$ s, the ground wave propagation is amplified by the wheel/defect contact due to the vehicle/track dynamics. This effect is visible until $t = 1$ s, showing that the phenomenon is transient and affects each wheel/defect impact. It is noteworthy that the embankment plays a role in the ground wave propagation by trapping wave guide for railway vibrations (clearly visible in Figures 7(c) and (d)). This results in increased vibration levels inside the embankment and was also found by Connolly, Giannopoulos and Forde (2013).

4.2. The influence of defect type

The six shapes of discontinuity presented in Figure 2 (representing various defect types such as transition zones, switches, crossings, rail joints, and wheel flats) are analysed in this section. Again, the vehicle is the AM96 trainset running at a constant speed v_0.

Figure 8 presents the surface ground vibration levels at different distances from the track, outside the embankment. The values of defect length and size were selected according to those found in practice. For the ramp function, the length l is 200 mm (sufficiently long to replicate a small transition zone with a slope of 3°) and height $h = 10$ mm. For the pulse function, the length is fixed at $l = 10$ mm with a height $h = 5$ mm. For the negative pulse function, the length is fixed at $l = 20$ mm. For the other rail defects, only the height intervenes, fixed to $h = 5$ mm. The wheel flat spot has a length $r = 50$ mm.

Although there is no similarity between the studied defects and dimensions, the results show large discrepancies between ground vibration levels. Furthermore, a difference in results is obtained between the step-up and step-down joint cases, despite the geometry being symmetrically identical. This difference is relatively high in the near field (e.g. at 8 m from the track, with a level twice greater for the step-up joint) but less pronounced in the far field (at 16 m, it is the opposite: the step-down joint induces largest vibrations). This is due to non-linear effects at the wheel/rail contact where climbing and dropping do not represent the same dynamic effect due to the absence of contact during dropping (the two defects are identical, but

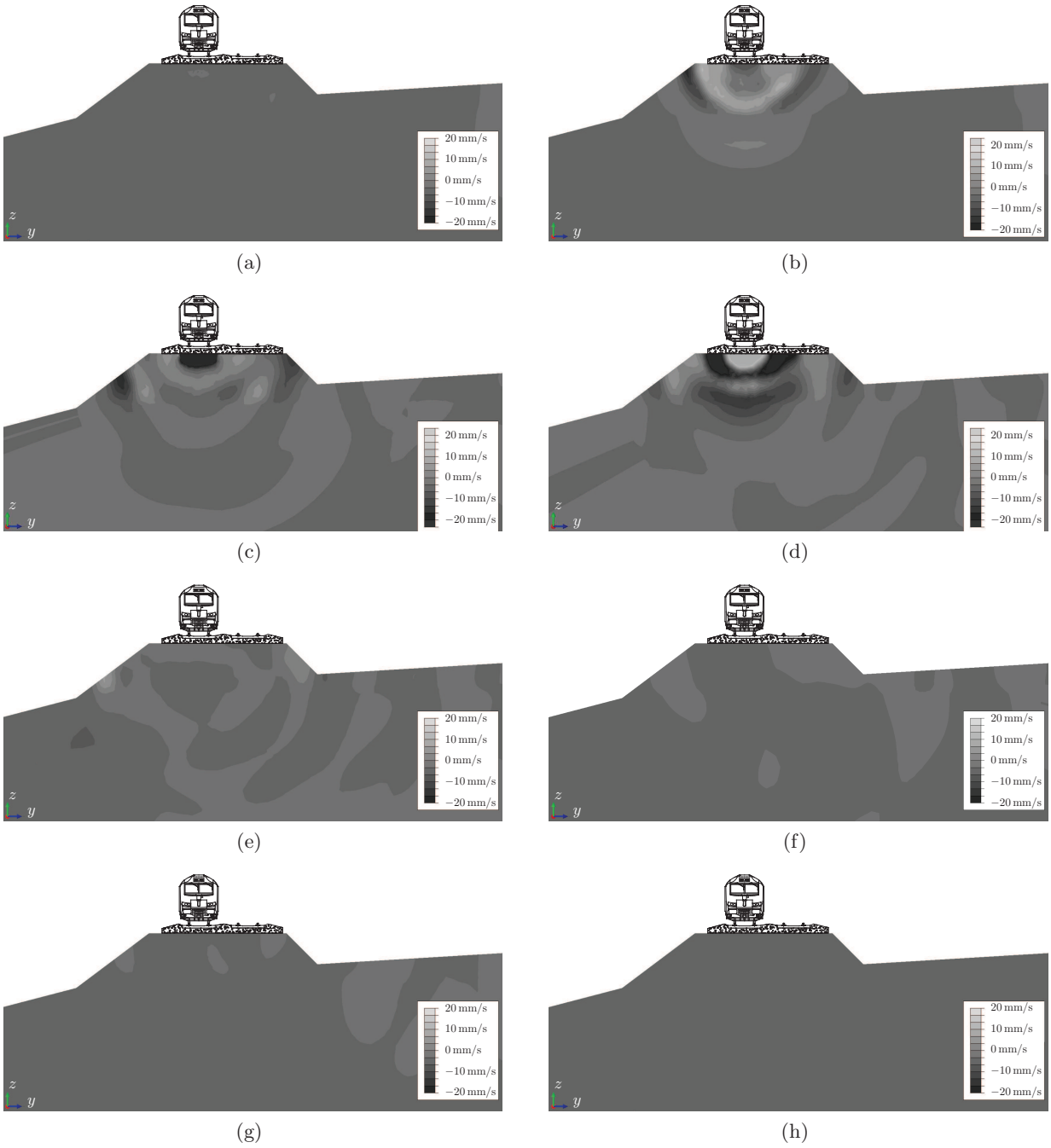

Figure 7. Numerical visualisation (x-axis planar view — vertical velocity v_z) of the passage of an AM96 trainset at a speed of 120 km/h on a 5 mm height ramp defect: free field vertical component of the soil vibration waves (a) at 0.7 s, (b) at 0.75 s, (c) at 0.8 s, (d) at 0.85 s, (e) at 0.9 s, (f) at 0.95 s, (g) at 1.0 s , (h) at 1.05 s.

opposite in shape). The ramp function also presents large vibration levels although it represents a priori a small variation in height. Very small levels of vibration are observed for the negative pulse and wheel flat, and are close to those obtained in the absence of local defects (not presented here). Finally, the decrease of vibration level with the distance is not the same for each defect and some small local increases in PPV

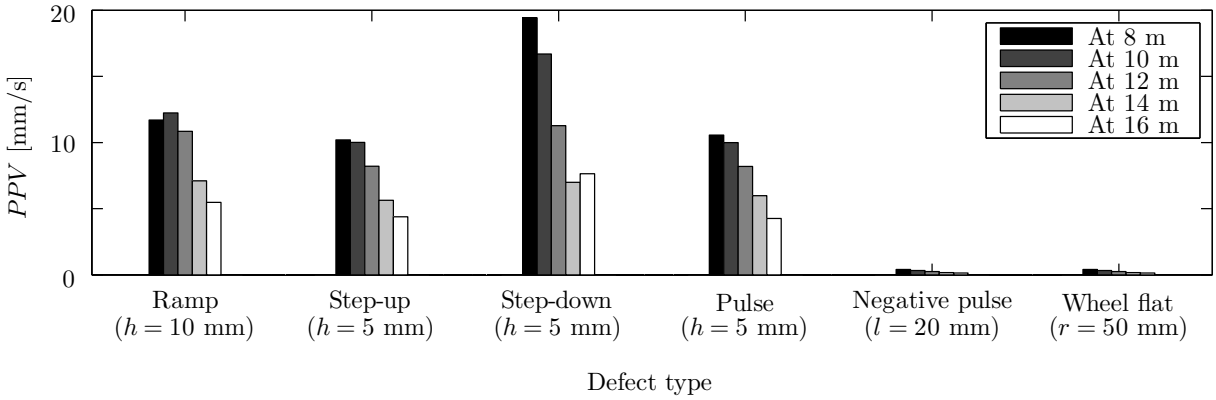

Figure 8. Peak particle velocity as a function of the distance from the source and the defect type for an AM96 trainset running at 120 km/h.

occur with distance.

4.3. The influence of defect size

A sensitivity analysis is presented in Tables 4 through 9 for when the primary defect dimension varies (h for the ramp, the step-up joint, the step-down joint, the pulse joint; l for the negative pulse joint; r for the wheel flat). The four aforementioned indicators (acceleration $\langle a_w \rangle$ and velocities PPV, $KB_{F,\max}$ and V_{dB}) are used to quantify the variation in ground vibration level. In general, there was found to be a positive relationship between each indicator and defect size. Despite this, the relationship between size and vibration level was not linear due to the non-linear effect of the wheel/rail contact. In addition, for some defects (e.g. step-down joint), the size was found to be very influential on defect size.

Table 4. Ground vibration level at 10 m from the source for an AM96 trainset running at 120 km/h on a ramp.

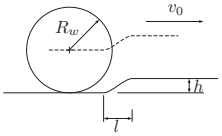

	$h = 5$ mm $l = 200$ mm	$h = 10$ mm $l = 200$ mm	$h = 15$ mm $l = 200$ mm
$\langle a_w \rangle$	0.37 m/s^2 (−56 %)	0.84 m/s^2	1.15 m/s^2 (+37 %)
$KB_{F,\max}$	2.26 mm/s (−57 %)	5.29 mm/s	7.22 mm/s (+36 %)
PPV	4.78 mm/s (−61 %)	12.23 mm/s	20.64 mm/s (+69 %)
V_{dB}	90.7 dB (−8 %)	98.1 dB	101.0 dB (+3 %)

Table 5. Ground vibration level at 10 m from the source for an AM96 trainset running at 120 km/h on a step-up joint.

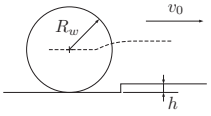

	$h = 2.5$ mm	$h = 5$ mm	$h = 7.5$ mm
$\langle a_w \rangle$	0.35 m/s^2 (−47 %)	0.67 m/s^2	0.78 m/s^2 (+17 %)
$KB_{F,\max}$	1.95 mm/s (−57 %)	4.54 mm/s	5.06 mm/s (+11 %)
PPV	4.29 mm/s (−57 %)	10.01 mm/s	11.43 mm/s (+14 %)
V_{dB}	89.8 dB (−7 %)	96.2 dB	97.3 dB (+1 %)

At 120 km/h, the wheel flat and negative pulse have an insignificant effect on ground vibrations. In general, this is due to the vehicle speed shifting the frequency content to a higher range. These high frequencies are then rapidly dampened by the soil and the track, meaning that, at the studied distances, their effect is insignificant. Figure 9 illustrates this by comparing the soil surface PPV generated by the train's passing (results observed for one side from the track). The same magnitude scale is used and shows

Table 6. Ground vibration level at 10 m from the source for an AM96 trainset running at 120 km/h on a step-down joint.

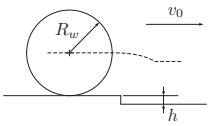

	$h = 2.5$ mm	$h = 5$ mm	$h = 7.5$ mm
$\langle a_w \rangle$	0.14 m/s^2 (−66 %)	0.42 m/s^2	0.88 m/s^2 (+108 %)
$KB_{F,\max}$	0.84 mm/s (−86 %)	6.22 mm/s	10.40 mm/s (+67 %)
PPV	2.13 mm/s (−87 %)	16.69 mm/s	28.49 mm/s (+71 %)
V_{dB}	81.7 dB (−15 %)	96.1 dB	102.2 dB (+6 %)

Table 7. Ground vibration level at 10 m from the source for an AM96 trainset running at 120 km/h on a pulse joint.

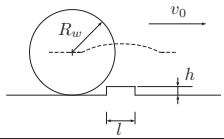

	$h = 2.5$ mm $l = 10$ mm	$h = 5$ mm $l = 10$ mm	$h = 7.5$ mm $l = 10$ mm
$\langle a_w \rangle$	0.36 m/s^2 (−51 %)	0.73 m/s^2	0.72 m/s^2 (−1 %)
$KB_{F,\max}$	1.93 mm/s (−57 %)	4.51 mm/s	4.50 mm/s (−0.1 %)
PPV	4.06 mm/s (−59 %)	10.00 mm/s	10.31 mm/s (+3 %)
V_{dB}	89.6 dB (−7 %)	96.5 dB	97.6 dB (+0.1 %)

Table 8. Ground vibration level at 10 m from the source for an AM96 trainset running at 120 km/h on a negative pulse joint.

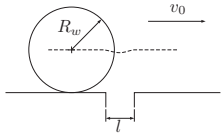

	$l = 10$ mm	$l = 20$ mm	$l = 30$ mm
$\langle a_w \rangle$	0.02 m/s^2 (+0.3 %)	0.02 m/s^2	0.02 m/s^2 (−0.7 %)
$KB_{F,\max}$	0.12 mm/s (+0.6 %)	0.12 mm/s	0.12 mm/s (−1 %)
PPV	0.32 mm/s (−0.4 %)	0.32 mm/s	0.32 mm/s (+1 %)
V_{dB}	66.9 dB (+0 %)	66.9 dB	66.8 dB (−0.2 %)

Table 9. Ground vibration level at 10 m from the source for an AM96 trainset running at 120 km/h with a wheel flat.

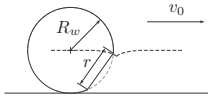

	$r = 20$ mm	$r = 30$ mm	$r = 40$ mm
$\langle a_w \rangle$	0.02 m/s^2 (−0.3 %)	0.02 m/s^2	0.02 m/s^2 (−0.1 %)
$KB_{F,\max}$	0.12 mm/s (+0.2 %)	0.12 mm/s	0.12 mm/s (+0.1 %)
PPV	0.32 mm/s (+0.5 %)	0.32 mm/s	0.32 mm/s (+0.5 %)
V_{dB}	66.9 dB (+0 %)	66.9 dB	66.9 dB (+0 %)

the difference between the different cases, as observed in the near-field embankment area. In Figure 9(a), the reference case without a defect is shown and Figure 9(b) shows the case for a defect generating large amplitude vibrations (5 mm height step-up joint defect). The negative pulse defect and wheel flat defect cases are also presented (Figures 9(c) and (d)) because there are associated to relatively low ground vibration levels. For both defects, the ground vibration level is very close to the reference case, except in the vicinity of the track where a discrepancy is found. This is because the periodic effect of wheel flat impact affects the track while the effect of the negative pulse defect affects a close area localised around the geometrical defect. Regarding the vibration field generated by the step-up joint defect, it is similar to those generated by a stationary point load (spherical-like ground wave shapes). Therefore this implies that the longitudinal position of the defect is important in the assessment of vibration annoyance in addition to distance from the track.

4.4. The influence of vehicle speed

Figure 10 presents, the variation in PPV for several distances from the track, for each defect, for speeds $v_0 = 100$ km/h, 120 km/h and 140 km/h. Note that the two defects — negative pulse joint and wheel flat — were not greatly effected by train speed (in these cases, the effect of speed is associated with the quasi-static

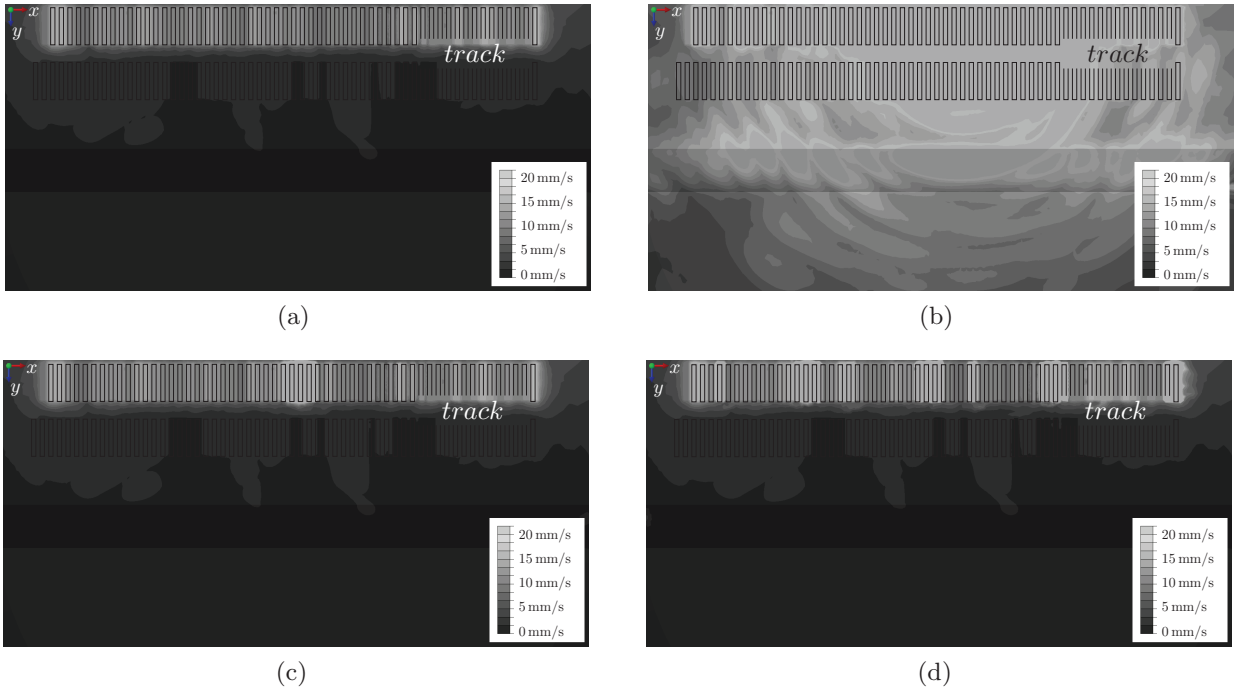

Figure 9. Birdseye track view (PPV according to Eq. (7)) during the passage of an AM96 trainset at a speed of 120 km/h (a) without defect (static contribution), (b) with a 5 mm height step-up joint defect, (c) with a 40 mm length negative pulse defect and (d) with a 50 mm flat spot.

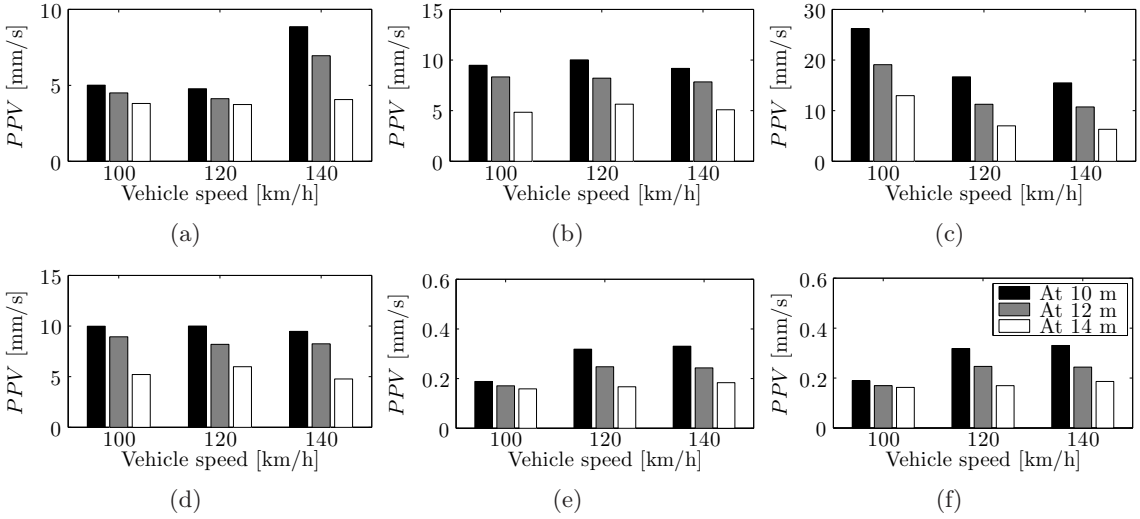

Figure 10. Peak particle velocity as a function of the vehicle speed for an AM96 trainset running on (a) ramp ($l = 200$ mm, $h = 5$ mm), (b) step-up joint ($h = 5$ mm), (c) step-down joint ($h = 5$ mm), (d) pulse joint ($h = 5$ mm), (e) negative pulse joint ($l = 10$ mm) and (f) wheel flat ($r = 50$ mm).

contribution of the vehicle only). Despite this, for some defects (e.g. ramp, negative pulse joint, wheel flat), higher vehicle speeds resulted in elevated ground vibration levels. For the other defects, the opposite was true and a negative relationship was found. The same observation (although not presented here) was found for all vibration indicators. This was interesting because commonly it is assumed that for rail irregularities,

vibration levels always increase with the vehicle speed. To understand this, it is useful to note that in previous studies, vibration levels were calculated using numerical and experimental observations where only quasi-static effects (moving load along the track) were coupled to a distributed overall unevenness (dynamic effect). In this case, local defects are considered rather than continuous defects, and thus generate different dynamic effects due to the contrast in the vehicle/track interaction. This changes the frequency response of the system, which may also be subject to carriage modulation effects (i.e. the frequency content generated by the defect impact may be magnified if it is inside the lobes defined by the axle periodicity).

5. Conclusion

The effect of railway track local irregularities (discontinuities) on ground-vibration levels was analysed. A time domain vibration prediction model was used to investigate vibration levels generated at the wheel/rail contact due to a variety of defects, including rail joints, switches, crossings and wheel flats. This was advantageous because when simulating transient events such as the forces generated in the contact zone between wheel and track discontinuities, time domain modelling is better suited than most frequency domain approaches. The prediction of 4 international metrics ($\langle a_w \rangle$, $KB_{F,\max}$, PPV and V_{dB}) was considered, and a sensitivity analysis was undertaken based upon the defect size and train speed. The key findings were:

- Local defects generate large amplitude excitations in comparison to a typical smooth railway track.
- The rate of vibration decay with the distance differs in the presence of a local defect. For the soil stratum modelled in this work, the decay rate was lower than that usually predicted by previous studies. Therefore it is possible for the vibrations from a defect to propagate to elevated distances in comparison to typical railway vibration
- Defect type has a significant influence on vibration levels. Step-down joints typically associated with switch/crossings generate the highest level of vibration, whereas negative pulse joints, and wheel flats generate the lowest.
- Defect geometry influences vibration levels and, in general, an increasing defect size causes increasing vibration levels.
- The relationship between defect type and train speed in complex. For some defects, vibration levels increase with speed, however for other types it decreases.

References

Alexandrou, G., Kouroussis, G. and Verlinden, O. (2015). A comprehensive prediction model for vehicle/track/soil dynamic response due to wheel flats, *Journal of Rail and Rapid Transit* **in press, doi: 10.1177/0954409715576015**.

Andersson, C. and Oscarsson, J. (1999). Dynamic train/track interaction including state-dependent track properties and flexible vehicle components, *Vehicle System Dynamics* **33**(supplement): 47–58.

Auersch, L. and Said, S. (2010). Attenuation of ground vibrations due to different technical sources, *Earthquake Engineering and Engineering Vibration* **9**: 337–344.

Chebli, H., Clouteau, D. and Schmitt, L. (2008). Dynamic response of high-speed ballasted railway tracks: 3D periodic model and in situ measurements, *Soil Dynamics and Earthquake Engineering* **28**(2): 118–131.

Connolly, D., Giannopoulos, A., Fan, W., Woodward, P. and Forde, M. (2013). Optimising low acoustic impedance backfill material wave barrier dimensions to shield structures from ground borne high speed rail vibrations, *Construction and Building Materials* **44**: 557–564.

Connolly, D., Giannopoulos, A. and Forde, M. C. (2013). Numerical modelling of ground borne vibrations from high speed rail lines on embankments, *Soil Dynamics and Earthquake Engineering* **46**: 13–19.

Connolly, D. P., Costa, P. A., Kouroussis, G., Galvín, P., Woodward, P. K. and Laghrouche, O. (2015). Large scale international testing of railway ground vibrations across europe, *Soil Dynamics and Earthquake Engineering* **71**: 1–12.

Connolly, D. P., Kouroussis, G., Laghrouche, O., Ho, C. and Forde, M. C. (2014). Benchmarking railway vibrations — track, vehicle, ground and building effects, *Construction and Building Materials* **in press, doi: 10.1016/j.conbuildmat.2014.07.042**.

Connolly, D. P., Kouroussis, G., Woodward, P. K., Costa, P. A., Verlinden, O. and Forde, M. C. (2014). Field testing and analysis of high speed rail vibrations, *Soil Dynamics and Earthquake Engineering* **67**: 102–118.

Connolly, D. P., Kouroussis, G., Woodward, P. K., Verlinden, O., Giannopoulos, A. and Forde, M. C. (2014). Scoping prediction of re-radiated ground-borne noise and vibration near high speed rail lines with variable soils, *Soil Dynamics and Earthquake Engineering* **66**: 78–88.

Costa, P. A., Calçada, R., Cardoso, A. S. and Bodare, A. (2010). Influence of soil non-linearity on the dynamic response of high–speed railway tracks, *Soil Dynamics and Earthquake Engineering* **30**(4): 221 – 235.

Costa, P. A., Calçada, R. and Cardoso, A. S. (2012). Influence of train dynamic modelling strategy on the prediction of track–ground vibrations induced by railway traffic, *Journal of Rail and Rapid Transit* **226**(4): 434–450.

Coulier, P., François, S., Degrande, G. and Lombaert, G. (2013). Subgrade stiffening next to the track as a wave impeding barrier for railway induced vibrations, *Soil Dynamics and Earthquake Engineering* **48**: 119–131.

Degrande, G. and Schillemans, L. (2001). Free field vibrations during the passage of a Thalys high-speed train at variable speed, *Journal of Sound and Vibration* **247**(1): 131–144.

Deutsches Institut für Normung (1999a). *DIN 4150-2: Structural vibrations — Part 2: Human exposure to vibration in buildings*.

Deutsches Institut für Normung (1999b). *DIN 4150-3: Structural vibrations — Part 3: Effects of vibration on structures*.

Galvín, P. and Domínguez, J. (2009). Experimental and numerical analyses of vibrations induced by high-speed trains on the Córdoba–Málaga line, *Soil Dynamics and Earthquake Engineering* **29**: 641–651.

Galvín, P., François, S., Schevenels, M., Bongini, E., Degrande, G. and Lombaert, G. (2010). A 2.5D coupled FE-BE model for the prediction of railway induced vibrations, *Soil Dynamics and Earthquake Engineering* **30**(12): 1500–1512.

Garinei, A., Risitano, G. and Scappaticci, L. (2014). Experimental evaluation of the efficiency of trenches for the mitigation of train-induced vibrations, *Transportation Research Part D: Transport and Environment* **32**(0): 303–315.

Grossoni, I., Iwnicki, S., Bezin, Y. and Gong, C. (2015). Dynamics of a vehicle–track coupling system at a rail joint, *Journal of Rail and Rapid Transit* **229**(4): 364–374.

International Organization for Standardization (2003). *ISO 2631-2: Mechanical vibration and shock — Evaluation of human exposure to whole-body vibration — Part 2: Vibration in buildings (1 to 80 Hz)*.

Kouroussis, G., Connolly, D. P. and Verlinden, O. (2014). Railway induced ground vibrations — a review of vehicle effects, *International Journal of Rail Transportation* **2**(2): 69–110.

Kouroussis, G., Conti, C. and Verlinden, O. (2013). Experimental study of ground vibrations induced by Brussels IC/IR trains in their neighbourhood, *Mechanics & Industry* **14**(02): 99–105.

Kouroussis, G., Conti, C. and Verlinden, O. (2014). Building vibrations induced by human activities: a benchmark of existing standards, *Mechanics & Industry* **15**(5): 345–353.

Kouroussis, G., Florentin, J. and Verlinden, O. (2015). Ground vibrations induced by intercity/interregion trains: A numerical prediction based on the multibody/finite element modeling approach, *Journal of Vibration and Control* **in press, doi: 10.1177/1077546315573914**.

Kouroussis, G., Gazetas, G., Anastasopoulos, I., Conti, C. and Verlinden, O. (2011). Discrete modelling of vertical track–soil coupling for vehicle–track dynamics, *Soil Dynamics and Earthquake Engineering* **31**(12): 1711–1723.

Kouroussis, G., Pauwels, N., Brux, P., Conti, C. and Verlinden, O. (2014). A numerical analysis of the influence of tram characteristics and rail profile on railway traffic ground-borne noise and vibration in the brussels region, *Science of the Total Environment* **482-483**: 452–460.

Kouroussis, G., Van Parys, L., Conti, C. and Verlinden, O. (2013). Prediction of ground vibrations induced by urban railway traffic: an analysis of the coupling assumptions between vehicle, track, soil, and buildings, *International Journal of Acoustics and Vibration* **18**(4): 163–172.

Kouroussis, G., Van Parys, L., Conti, C. and Verlinden, O. (2014). Using three-dimensional finite element analysis in time domain to model railway–induced ground vibrations, *Advances in Engineering Software* **70**: 63–76.

Kouroussis, G. and Verlinden, O. (2015). Prediction of railway ground vibrations: accuracy of a coupled lumped mass model for representing the track/soil interaction, *Soil Dynamics and Earthquake Engineering* **69**: 220–226.

Kouroussis, G., Verlinden, O. and Conti, C. (2012). Efficiency of resilient wheels on the alleviation of railway ground vibrations, *Journal of Rail and Rapid Transit* **226**(4): 381–396.

Madshus, C. and Kaynia, A. M. (2000). High-speed railway lines on soft ground: dynamic behaviour at critical train speed, *Journal of Sound and Vibration* **231**(3): 689–701.

Mandal, N. K., Dhanasekar, M. and Sun, Y. Q. (2014). Impact forces at dipped rail joints, *Journal of Rail and Rapid Transit* **in press, doi: 10.1177/0954409714537816**.

Nielsen, J. C. O. and Abrahamsson, T. J. S. (1992). Coupling of physical and modal components for analysis of moving non-linear dynamic systems on general beam structures, *International Journal for Numerical Methods in Engineering* **33**(9): 1843–1859.

Nielsen, J. C. O., Mirza, A., Cervello, S., Huber, P., Müller, R., Nelain, B. and Ruest, P. (2015). Reducing train-induced ground-borne vibration by vehicle design and maintenance, *International Journal of Rail Transportation* **3**(1): 17–39.

Oscarsson, J. and Dahlberg, T. (1998). Dynamic train/track/ballast interaction - computer models and full-scale experiments, *Vehicle System Dynamics* **29**(supplement): 73–84.

Paixão, A., Fortunato, E. and Calçada, R. (2015). Design and construction of backfills for railway track transition zones, *Journal of Rail and Rapid Transit* **229**(1): 58–70.

Schweizerische Normen-Vereinigung (1992). *SN-640312a: Les ébranlements — Effet des ébranlements sur les constructions [Swiss Standard on vibration effects on buildings]*.

Sheng, X., Jones, C. J. C. and Thompson, D. J. (2006). Prediction of ground vibration from trains using the wavenumber finite and boundary element methods, *Journal of Sound and Vibration* **293**(3–5): 575–586.

Talbot, J. P. (2014). Lift-over crossings as a solution to tram-generated ground-borne vibration and re-radiated noise, *Journal of Rail and Rapid Transit* **228**(8): 878–886.

U. S. Department of Transportation (1998). High-speed ground transportation. Noise and vibration impact assessment, *Technical Report 293630–1*, Office of Railroad Development Washington (Federal Railroad Administration).

Uzzal, R. U. A., Ahmed, W. and Bhat, R. B. (2014). A three-dimensional modeling study of wheel/rail impacts created by multiple wheel flats, and the development of a smart wheelset, *Journal of Rail and Rapid Transit* **in press, doi: 10.1177/0954409714545558**.

Verlinden, O., Ben Fekih, L. and Kouroussis, G. (2013). Symbolic generation of the kinematics of multibody systems in EasyDyn: from MuPAD to Xcas/Giac, *Theoretical & Applied Mechanics Letters* **3**(1): 013012.

Vogiatzis, K. (2010). Noise and vibration theoretical evaluation and monitoring program for the protection of the Ancient "Kapnikarea Church" from Athens metro operation, *International Review of Civil Engineering* **1**: 328–333.

Vogiatzis, K. (2012). Protection of the cultural heritage from underground metro vibration and ground-borne noise in Athens centre: The case of the Kerameikos archaeological museum and Gazi cultural centre, *International Journal of Acoustics and Vibration* **17**: 59–72.

Younesian, D., Marjani, S. R. and Esmailzadeh, E. (2014). Importance of flexural mode shapes in dynamic analysis of high-speed trains traveling on bridges, *Journal of Vibration and Control* **20**(10): 1565–1583.

Zhai, W. and Sun, X. (1994). A detailed model for investigating vertical interaction between railway vehicle and track, *Vehicle System Dynamics* **23**(supplement): 603–615.

Zhai, W., Xia, H., Cai, C., Gao, M., Li, X., Guo, G., Zhang, N. and Wang, K. (2013). High-speed train–track–bridge dynamic interactions — Part I: theoretical model and numerical simulation, *International Journal of Rail Transportation* **1**(1-2): 3–24.

Zhao, X., Li, Z. and Liu, J. (2012). Wheel–rail impact and the dynamic forces at discrete supports of rails in the presence of singular rail surface defects, *Journal of Rail and Rapid Transit* **226**(2): 124–139.